Xie, Boxuan; Wang, Xiyu; Yiğitler, Hüseyin; Ruttik, Kalle; Jäntti, Riku

A Three-State Received Signal Strength Model for Integrated Sensing and Backscatter Communication

Published in:
2023 IEEE Globecom Workshops, GC Wkshps 2023

DOI:
10.1109/GCWkshps58843.2023.10465190

Published: 21/03/2024

Document Version
Peer-reviewed accepted author manuscript, also known as Final accepted manuscript or Post-print

Please cite the original version:
Xie, B., Wang, X., Yiğitler, H., Ruttik, K., & Jäntti, R. (2024). A Three-State Received Signal Strength Model for Integrated Sensing and Backscatter Communication. In *2023 IEEE Globecom Workshops, GC Wkshps 2023* (pp. 98-103). (2023 IEEE Globecom Workshops, GC Wkshps 2023). IEEE. https://doi.org/10.1109/GCWkshps58843.2023.10465190

A Three-State Received Signal Strength Model for Integrated Sensing and Backscatter Communication

Boxuan Xie, Xiyu Wang, Hüseyin Yiğitler, Kalle Ruttik, Riku Jäntti
Department of Information and Communications Engineering, Aalto University, 02150 Espoo, Finland
Email: {firstname.lastname}@aalto.fi

***Abstract*— Backscatter communication (BC) can enable narrowband radio frequency (RF) sensing with lower power consumption and lower system complexity compared with conventional sensing systems with active transmitter-receiver (TX-RX) pairs. To integrate sensing in the BC scenario, this paper investigates the impact of human position on the received signal strength (RSS). We first derive a new RSS model for the BC scenario based on three states: non-fading, reflection, and shadowing, depending on the location of the person with respect to line-of-sight (LoS) link. We validate the model by indoor measurements and compare it with the three-state model of the active TX-RX scenario. The measurements show that the proposed model accurately predicts human-induced RSS changes. Furthermore, we observe that human-induced RSS variances in the BC scheme are higher than those in the TX-RX scenario, benefiting variance-based sensing methods. Therefore, the proposed model can be implemented in low-power BC-enabled device-free sensing applications, such as human presence detection and device-free localization.**

***Index Terms*—Backscatter communication, received signal strength, human presence detection, device-free localization.**

I. Introduction

Human motion and activities interfere with electromagnetic (EM) wave propagation of wireless communication systems. This human-induced variation in the EM field exhibits different patterns depending on human actions. In beyond 5G (B5G) era, sensing and communication will coexist and be integrated into one system, known as integrated sensing and communication (ISAC) [1]. In the ISAC system, by extracting useful information from captured signals, one can realize device-free sensing. Available solutions exploit the Wi-Fi channel state information (CSI) [2], frequency modulated continuous wave (FMCW) radar [3], radio frequency identification (RFID) [4], and reconfigurable intelligent surface (RIS) [5] for device-free localization (DFL) and human presence detection (HPD). Among the DFL and HPD systems, backscattering radio methods are gaining prominence thanks to the ubiquitous deployment of ambient Internet-of-Things (AIoT) that is currently under discussion in the standardization of mobile networks [6], [7].

The sensing system integrated into conventional wireless sensor networks (WSNs) localizes or detects a person through coherent reception with received signal strength (RSS) and phase information. For acceptable performance, they need high-power transmissions and/or multiple active sensor nodes [8]. Integrating sensing with backscatter communication (BC) replaces active nodes with nearly passive backscatter tags and only one active transmitter-receiver (TX-RX) pair [9]. Backscatter tags modulate ambient RF signals transmitted from the TX. The RX then detects reflected signal from the tags, extracts RSS information and from there makes localization inferences. Thus, compared with the conventional WSN sensing with all active nodes, the BC-enabled ISAC systems consume orders of magnitude less power.

A moving human body alters radio propagation links and changes the RSS. The induced RSS variations are widely employed for sensing systems. In conventional WSNs with TX-RX pairs, a spatial model of RSS variance [8] is used for inferring human location. The human position, size, orientation, and movement around the radio link are related to a multi-body diffraction-based RSS model [10]. Human motions can be depicted from its induced RSS fading model [11], and the period of motion or stationary is estimated with a reciprocal RSS model [12]. These works demonstrate that RSS models are essential for different sensing problems. However, the above models were developed for conventional WSNs. In the BC-enabled ISAC scenario, investigations of RSS models are needed as the propagation link in BC systems is different. Moreover, before diving into sensing problems, this paper accurately models the RSS affected by a person and their location, which lays the foundation for localization.

The impact of a human body on RSS between an active TX-RX pair is thoroughly studied in [13] where a three-state model (3SM) as a function of the distance between the body and the line-of-sight (LoS) link is presented. We apply a similar modeling approach. In our proposed BC-enabled sensing scheme, radio propagation links contain reflectors, i.e., backscatter tags, which increase the human-induced multipath components. We model the human body impact on the BC propagation links, which is expressed by the RSS variations.

This paper models the impact of a human body on the RSS in a low-complexity indoor BC scheme. We consider that different backscatter tags modulate the impinging signal with different on/off speeds. This shifts the frequencies of the backscattered signal, resembling frequency modulation. Consequently, the RX can separate the backscatter signal using band-pass filters and record their RSS for further analysis.

This work makes the following contributions:

- We propose a BC-enabled ISAC system structure with experimental demonstration;
- We derive and characterize a human body location-dependent three-state RSS model (3SM-BC) for the BC

scheme;

- We validate the model by indoor measurement and compare it with the prior model (3SM) of the TX-RX scheme.

The results show that the proposed model accurately predicts human-induced RSS changes in the BC scenario. Hence, one can detect and localize the person using the RSS measurements. Moreover, compared with the conventional TX-RX schemes, extra propagation paths existing in the BC scheme lead to larger RSS variances, which can improve human detection and localization accuracy in variance-based sensing systems.

The rest of the paper is organized as follows. Section II proposes a BC-enabled ISAC system structure. Section III derives the spatial RSS model in terms of three different states. The proposed model is experimentally validated and compared with the existing model in Section IV. Finally, Section V concludes and discusses future work.

II. System Model

Let us consider a BC-enabled sensing system that includes an ambient carrier wave (CW) source, a receiver (RX), and several backscatter devices (BDs) composed of backscatter tags and microcontroller units. The BDs shift the frequency of the impinging CW and backscatter it to the RX. The RX receives samples containing both the CW and backscattered (BS) signals with different frequencies. By switching between two states of a BD with a certain frequency, the center frequency of the BS (tag-modulated path) is shifted away from the CW (direct path) by the amount of switching frequency [14]. The BS signal from a certain BD can be extracted by band-pass filtering while the CW signal and BS signals from other BDs are canceled out. In the following, we consider the scenario with only one BD to investigate the RSS variation of the received BS signal.

As shown in Fig. 1, we denote $\boldsymbol{p}_{CW}$, $\boldsymbol{p}_{BD}$ and $\boldsymbol{p}_{RX}$ as the positions of the CW source, BD, and RX, respectively. We consider a common BC configuration, bistatic collocated BC, where the CW source and RX are collocated. It is similar to mono-static BC configuration but it avoids using the complicated full-duplex transceivers. Let the center of two devices, denoted by $\boldsymbol{p}_o$, approximates their positions, i.e., $\boldsymbol{p}_0 \approx \boldsymbol{p}_{CW}$ and $\boldsymbol{p}_0 \approx \boldsymbol{p}_{RX}$. In the following, we use X-Y to express the radio propagation path from one device X to another device Y. We first define the LoS link of the BC system as LoS_{BC} which is composed of $\text{LoS}_{\text{CW-BD}}$ link and $\text{LoS}_{\text{BD-RX}}$ link. The LoS_{BC} has a distance

$$d_{LoS} = \|\boldsymbol{p}_{CW} - \boldsymbol{p}_{BD}\| + \|\boldsymbol{p}_{RX} - \boldsymbol{p}_{BD}\| \approx 2d, \quad (1)$$

where $\|\cdot\|$ is Euclidean norm. For the indoor BC scenario, we assume that the communication system only experiences slow fading due to the movement of a person, similar to other indoor DFL systems [15]. When a person appears in the vicinity of the LoS link, there adds some more reflected multipath components receiving at the RX. Then, excess path length caused by the human body, denoted by Δ, describes the signal propagating a longer distance with a time delay and a phase shift compared with the LoS link. In the BC system, excess path length exists on both CW-BD and BD-RX links, denoted by Δ_{CW} and Δ_{BS}, respectively, and are defined as

$$\begin{aligned} \Delta_{CW} &= \|\boldsymbol{p} - \boldsymbol{p}_{CW}\| + \|\boldsymbol{p} - \boldsymbol{p}_{BD}\| - d, \\ \Delta_{BS} &= \|\boldsymbol{p} - \boldsymbol{p}_{RX}\| + \|\boldsymbol{p} - \boldsymbol{p}_{BD}\| - d, \end{aligned} \quad (2)$$

where $\boldsymbol{p} = [p_x \ p_y]^T$ is the position of the human. Because the CW and RX are sufficiently close, we approximate both Δ_{CW} and Δ_{BS} to

$$\Delta = \|\boldsymbol{p} - \boldsymbol{p}_o\| + \|\boldsymbol{p} - \boldsymbol{p}_{BD}\| - d. \quad (3)$$

In general, multipath components created by the human body add constructive or destructive fading to the LoS_{BC} channel. Hence, the RSS observed by the RX varies depending on Δ, and in other words, on the person's location. In order to investigate human-induced RSS variation in the BC-enabled sensing system, we only take the BS signal into account. To do that, we use band-pass filtering to extract the BS signal from received samples, where the CW and BS signals are separated in the frequency domain. In addition, we remove the mean of the RSS so as to remove the parts that depend on the communication system and environment, and resultant RSS variations reflect the changes caused by the presented person. Let $R(k)$ denotes a temporal RSS measurement at time instance k, and $\overline{R}$ is the reference or baseline RSS when no person is present in the monitoring area, shown in Fig. 1. Thus, the mean-removed RSS in the logarithmic scale is expressed by

$$r(k) = R(k) - \overline{R}. \quad (4)$$

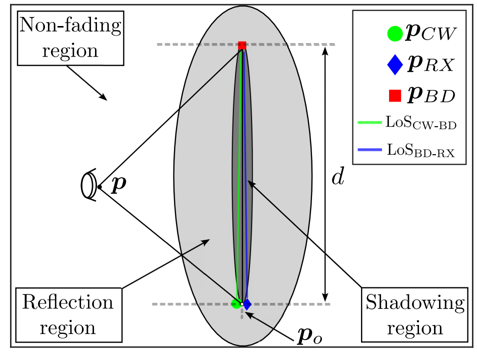

Fig. 1. Proposed BC system and its three-state regions.

III. The Spatial RSS Model

In the proposed BC system, RSS variations of BS signal can be modeled with three temporal states [13], i.e., *non-fading* when the person is far away from the LoS_{BC} link, *reflection* when the person is in the vicinity of the link, and *shadowing* when the person is blocking the link. The mean-removed RSS depending on the state s is defined as follows:

$$r(k) = \begin{cases} \mathcal{N}(k) + v(k) & s = s_1(\text{Non-fading}), \\ \mathcal{R}(k) + v(k) & s = s_2(\text{Reflection}), \\ \mathcal{S}(k) + v(k) & s = s_3(\text{Shadowing}), \end{cases} \quad (5)$$

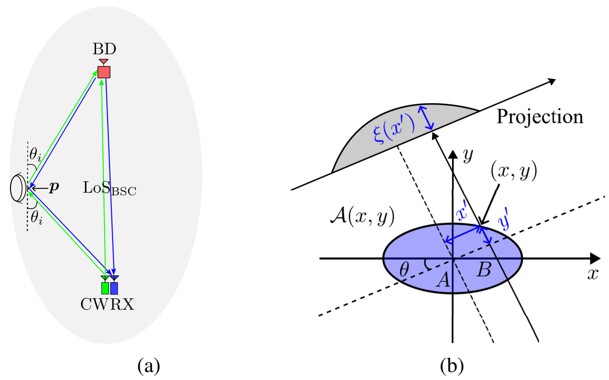

Fig. 2. Spatial model: (a) reflection, (b) shadowing.

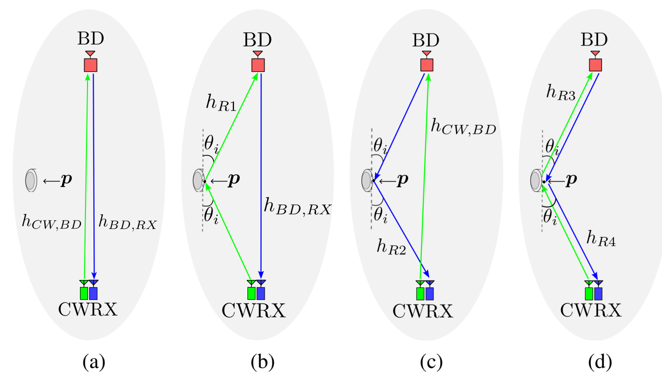

Fig. 3. Propagation paths decomposition: (a) LoS_{BC} channel, (b)-(d) human-induced reflection channels.

where $\mathcal{N}(k)$, $\mathcal{R}(k)$, and $\mathcal{S}(k)$ are the models in non-fading, reflection, and shadowing state in their respective order, and $v(k)$ is the additive-white-Gaussian-noise. In this section, the spatial RSS models are derived for each state.

A. Non-fading State

This state depicts that a person presents outside of the sensitivity region of the LoS_{BC} shown in Fig. 1. In this state, the RSS variation is too weak to be observed in the propagation medium such that $\mathcal{N}(k) = 0$, and $r(k)$ follows statistics of $v(k)$.

B. Reflection State

When the person is moving in the vicinity of the LoS_{BC} shown in Fig. 2a, both CW and BS signals are reflected from the surface of the dielectric target, creating several clusters of additional multipath components. In this state, as shown in Figures 3a to 3d, the channel may experience four propagation paths. They are: a). the LoS_{BC} with few interference created by the human body; b). the CW is reflected at the human body and is captured by the BD, which is then modulated, backscattered, and received by the RX; c). the CW is first captured, modulated, and backscattered by the BD, and is then reflected at the human body, which is finally received by the RX; d). both the CW and BS signals are reflected at the human body and are then received by the RX. In the following, we describe and analyze the four types of channel propagation individually.

1) LoS_{BC} propagation path: The CW source emits a carrier wave $c(k) = Ce^{j2\pi f_c k}$ with an amplitude C and a carrier frequency f_c at the time instance k. Assume the $\text{LoS}_{\text{CW-BD}}$ has a constant channel gain $h_{CW,BD} = \alpha_{CW,BD}e^{-j\phi_{CW,BD}}$ with an amplitude $\alpha_{CW,BD}$ and a phase $\phi_{CW,BD}$, so that the BD receives

$$a(k) = h_{CW,BD} \circledast c(k) = \alpha_{CW,BD}e^{-j\phi_{CW,BD}} \cdot c(k), \quad (6)$$

where the $\circledast$ denotes convolution. Then, the BD modulates its baseband signal $x(k)$ on top of its received signal $a(k)$ yielding the signal backscattered from the BD as $b(k) = x(k) \cdot a(k)$. Similarly, assume the $\text{LoS}_{\text{BD-RX}}$ has a constant channel gain $h_{BD,RX} = \alpha_{BD,RX}e^{-j\phi_{BD,RX}}$. Finally, the RX receives

$$y(k) = h_{BD,RX} \circledast b(k) = \alpha_{BD,RX}e^{-j\phi_{BD,RX}} \cdot b(k). \quad (7)$$

The channel gains of the $\text{LoS}_{\text{CW-BD}}$ and $\text{LoS}_{\text{BD-RX}}$ are assumed to be approximately identical because of the short distance, i.e., $\alpha_{CW,BD} \approx \alpha_{BD,RX} = \alpha_{LoS}$. The BD is assumed to be synchronized to the $\text{LoS}_{\text{CW-BD}}$ components and the RX is assumed to be synchronized to the $\text{LoS}_{\text{BD-RX}}$ components, resulting in $\phi_{CW,BD} = \phi_{BD,RX} = 0$. Thus, the RX received signal which experiences the LoS_{BC} can be expressed by

$$y_0(k) = \alpha_{LoS}^2 \cdot c(k) \cdot x(k). \quad (8)$$

Further, the channel gain that affects RSS measurements w.r.t. signal power is expressed by

$$|h_0(k)|^2 = \left|\alpha_{LoS}^2\right|^2, \quad (9)$$

which indicates the person has few effects on measured RSS, resembling the non-fading channel. Therefore, the channel is only depicted by the stochastic noise, shown in Fig. 3a.

2) Human-induced reflection, CW-Person-BD-RX: Assume the BD received CW signal experiences the reflection channel with a gain $h_{R1}(k) = \alpha_{R1}(k)e^{-j\phi_{R1}(k)}$. Thus, the RX received signal is expressed by

$$y_1(k) = \alpha_{LoS} \cdot \alpha_{R1}(k)e^{-j\phi_{R1}(k)} \cdot c(k) \cdot x(k). \quad (10)$$

The channel gain that affects RSS measurements w.r.t. signal power can be calculated by

$$|h_1(k)|^2 = \left|\alpha_{LoS} \cdot \alpha_{R1}(k)e^{-j\phi_{R1}(k)}\right|^2, \quad (11)$$

which indicates the radio propagation path shown in Fig. 3b.

3) Human-induced reflection, CW-BD-Person-RX: Assume the RX received BS signal experiences the reflection channel with a gain $h_{R2}(k) = \alpha_{R2}(k)e^{-j\phi_{R2}(k)}$. Thus, the RX received signal can be expressed by

$$y_2(k) = \alpha_{LoS} \cdot \alpha_{R2}(k)e^{-j\phi_{R2}(k)} \cdot c(k) \cdot x(k). \quad (12)$$

The channel gain that affects RSS measurements w.r.t. signal power can be calculated by

$$|h_2(k)|^2 = \left|\alpha_{LoS} \cdot \alpha_{R2}(k)e^{-j\phi_{R2}(k)}\right|^2, \quad (13)$$

which indicates the radio propagation path shown in Fig. 3c.

4) Human-induced reflection, CW-Person-BD-Person-RX: Similarly, assume the BD received CW signal and the RX received BS signal experiences the reflection channel $\alpha_{R3}(k)e^{-j\phi_{R3}(k)}$ and $\alpha_{R4}(k)e^{-j\phi_{R4}(k)}$, respectively. Thus, the RX received signal can be expressed by

$$y_3(k) = \alpha_{R3}(k)e^{-j\phi_{R3}(k)} \cdot \alpha_{R4}(k)e^{-j\phi_{R4}(k)} \cdot c(k) \cdot x(k). \quad (14)$$

The channel gain that affects RSS measurements w.r.t. the signal power can be calculated by

$$|h_3(k)|^2 = \left|\alpha_{R3}(k)e^{-j\phi_{R3}(k)} \cdot \alpha_{R4}(k)e^{-j\phi_{R4}(k)}\right|^2, \quad (15)$$

which indicates the radio propagation path shown in Fig. 3d.

Therefore, the received signals listed above can be summed at the RX side and then become

$$y(k) = y_0(k) + y_1(k) + y_2(k) + y_3(k), \quad (16)$$

with a total channel gain

$$|h(k)|^2 = |h_0(k) + h_1(k) + h_2(k) + h_3(k)|^2. \quad (17)$$

Here, all the reflection channels are assumed to be approximately identical due to static indoor environment, i.e.,

$$\begin{cases} \alpha_{R1}(k) \approx \alpha_{R2}(k) \approx \alpha_{R3}(k) \approx \alpha_{R4}(k) = \alpha_R(k), \\ \phi_{R1}(k) \approx \phi_{R2}(k) \approx \phi_{R3}(k) \approx \phi_{R4}(k) = \phi_R(k). \end{cases} \quad (18)$$

Therefore, the reflected signal can be expressed w.r.t. the LoS signals with the aforementioned synchronization condition and slow-fading environment, the total channel gain can be simplified by

$$|h(k)|^2 = \left|\alpha_{LoS}^2 \cdot (1 + \Lambda e^{-j\phi_R(k)})^2\right|^2, \quad (19)$$

where $0 < \Lambda = \alpha_R(k)/\alpha_{LoS} < 1$ indicates the relation between α_{LoS} and $\alpha_R(k)$, which is defined by $\Lambda \triangleq \gamma \left(d_{LoS}/(d_{LoS} + \Delta)\right)^{\eta/2}$, where η is experiment dependent and time-invariant path loss coefficient and γ is time-variant *Fresnel reflection coefficient* of vertical electric field polarization at the boundary of two dielectrics

$$\gamma = \frac{\sin\theta_i - \sqrt{\varepsilon_r - \cos^2\theta_i}}{\sin\theta_i + \sqrt{\varepsilon_r - \cos^2\theta_i}}, \quad (20)$$

where ε_r is relative permittivity, and θ_i is incident angle of reflection. The mean of RSS is removed in logarithmic scale that is equivalent to division in linear scale. Thus, the reflection model is expressed by

$$\begin{aligned} \mathcal{R}(k) &= 10\log_{10}\left(\frac{|h(k)|^2}{|h_0(k)|^2}\right) \\ &= 20\log_{10}(\Lambda^2 + 2\Lambda\cos\phi_R(k) + 1). \end{aligned} \quad (21)$$

C. Shadowing State

When the person is approximately blocking the LoS_{BC}, there exists reflection, diffraction, and scattering of EM waves which makes it difficult to accurately model the physical propagation scheme. Using the *Radon transform* [13], a simplification can be implemented by assuming transmission through the human body predominates the propagation, where the resulting signal attenuation is expressed by a line integral of the attenuation area along a straight line from the BD to the center of the CW source and RX, shown in Fig. 2b, given by $y' = x\cos(\theta) + y\sin(\theta) - x'$. The total attenuation is then

$$\xi(x') = n\int_{-\infty}^{\infty}\int_{-\infty}^{\infty} \mathcal{A}(x,y)\delta\left(x\cos\theta + y\sin\theta - x'\right)dxdy, \quad (22)$$

where $\delta(\cdot)$ is *Dirac function*, and $\mathcal{A}(x,y)$ is attenuation factor. The human cross section is modeled as an ellipse with uniform electrical properties, i.e., $\mathcal{A}(x,y) = \mathcal{A}$. It is worth noting that the coefficient n indicates the attenuation caused by the n blocked LoS paths. In the considered BC scenario, $n = 2$ due to attenuation at both the $\text{LoS}_{\text{CW-BD}}$ and $\text{LoS}_{\text{BD-RX}}$. With such properties, the closed-form solution for Eq.(22) is

$$\xi(x') = \begin{cases} \mathcal{A}\frac{4AB}{a^2(\theta)}\sqrt{a^2(\theta) - (x')^2} & \text{if } |x'| \le a(\theta), \\ 0 & \text{otherwise}, \end{cases} \quad (23)$$

where A and B are the semi-minor and semi-major axis of the human ellipse that has a relation $a^2(\theta) = A^2\cos^2(\theta) + B^2\sin^2(\theta)$. From the experiments, larger attenuation is observed when the human target walks along the paths that are closer to the devices, which phenomenon can be explained by the propagation *Fresnel zone* that are concentric ellipsoids with radius $d_n = \sqrt{(n\lambda d_{BD}d_o)/(d_{BD} + d_o)}$, where n is the number of the Fresnel zone, λ denotes the wavelength, d_{BD} and d_o are the distances from the human body to the BD and to the center of CW source and RX, respectively. For the considered scenario, shadowing occurs only inside the first Fresnel zone, so that the relation can be expressed by the width of the person divided by the first Fresnel zone radius, i.e., A/d_1. Besides, the motion of the human elliptic model is defined w.r.t. the radio link so that $\theta = 0$ and $x' = p_x$. Therefore, the decreasing of RSS measurement is equivalent to accumulating the attenuation along the LoS_{BC} propagation path, so that the shadowing model is expressed by

$$\mathcal{S}(k) = -\frac{A}{d_1}\xi(p_x). \quad (24)$$

IV. Experiment and Empirical Validation

In this section, the proposed RSS model is validated in the BC system introduced in Sec. II, and is compared with the prior three-state model that only considers the TX-RX transmission scheme. A Rohde & Schwarz SGT100A signal generator sends 2.4 GHz continuous sine-wave as the CW source signal, and a software-defined radio receiver USRP X300 with 1 MHz sampling rate is deployed with a distance of 12.5 cm, whose antennas (CW and RX1) are placed at 1.0 m height tripods, and are set 3.0 m apart from the BD. We use the BD introduced in [16]. In order to compare the proposed model and measurements with those of the prior TX-RX scenario, another receiving antenna (RX2) is collocated with the BD to measure the RSS of the TX-RX2 radio link. Both receiving antennas are connected to the USRP yet separated ports and channels.

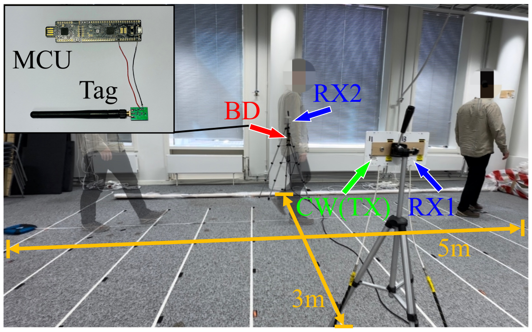

Fig. 4. Experimental setup and measurement collection.

TABLE I
EXPERIMENTAL PARAMETERS

Parameter	Value	Description
ε_r	1.5	Relative permittivity
η	2.0	Path loss coefficient
A	0.14	Semi-minor axis of the human model (m)
B	0.16	Semi-major axis of the human model (m)
$\mathcal{A}$	80.0	Attenuation factor (dB/m)

The experimental setup and a demonstration of measurement collections when a person is walking in the monitoring area are shown in Fig. 4. The space is a $5 \times 3 = 15$ m^2 corridor. The person walks along the trajectory with markers pasted on the floor, following a metronome with a preset pace of 0.5 m/s, intersecting the $\mathrm{LoS_{BC}}$ with multiple repetitions. In total, $2.4 \cdot 10^4$ RSS measurements are collected. The model-related experimental parameters are listed in Tab. I, which are experiment dependent. The relative permittivity ε_r of commonly used textile materials is around 1.5 at 2.4 GHz band [17]. The semi-minor and -major axes of the human model are used according to the participant's body. The path loss coefficient η and attenuation factor $\mathcal{A}$ follow those in our prior work [13] because of the similar indoor radio propagation environment. In practical applications, online training algorithms such as expectation maximization can be used to estimate model parameters, which will not be discussed in this paper.

In Fig. 5a, the RSS measurements corresponding to the three states proposed in Sec. III are observed. The RSS recorded from the RX1 (red circles) indicating the BC scenario, and from the RX2 (blue circles) indicating the TX-RX scenario, are shown together for comparison. For each time instance k, samples from twelve experiment repetitions are shown together. The time instance $k = 0$ is mapped to the beginning of the walking trajectory and $k = 1000$ is mapped to the ending of it. The state s_1 is observed at samples $k = [0, 350]$ and $k = [670, 1000]$ which indicates the person is in the non-fading region. The state s_2 is observed at samples $k = [350, 480]$ and $k = [540, 670]$ which indicates the person is in the reflection region, and the state s_3 is observed at samples $k = [480, 540]$ which indicates the person is moving in the shadowing region. Here, boundaries of the regions are manually defined by

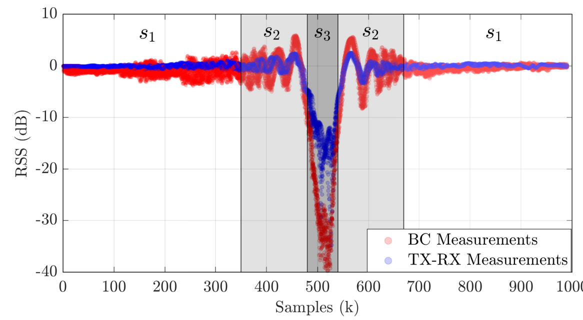

(a)

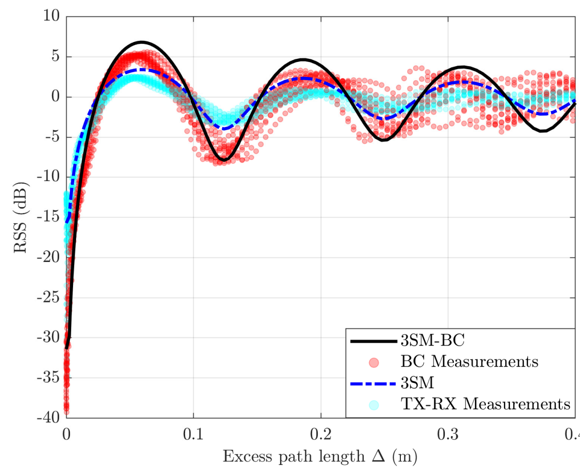

(b)

Fig. 5. Empirical validation and comparison: (a) RSS measurements corresponding to the three states, (b) spatial RSS models and measurements.

observation, which also can be defined using the statistical hypothesis testing method in [13]. It can be seen that RSS measurements of the BC scenario follow a similar variation pattern to that of the TX-RX scenario. Furthermore, for the BC scenario, RSS measurements have larger variations in terms of amplitude and have larger fading as the person blocking the LoS.

The model-predicted RSS variations with the increasing excess path length Δ for the derived model (3SM-BC) and the prior three-state model (3SM) are compared and shown in Fig. 5b. The proposed model 3SM-BC shows a similar pattern of RSS variation compared with the 3SM. However, the RSS in the reflection state of the 3SM-BC is expected to be double that of the 3SM due to multiple reflections, recalling Eq.(21). Similarly, the RSS in the shadowing state of the 3SM-BC is expected to be double that of the 3SM due to the superposition of attenuation, recalling Eq.(22).

To evaluate the model accuracy, the root-mean-square error (RMSE) measuring the difference between the model-predicted and the measured RSS values is used, given by

$$RMSE = \sqrt{\frac{1}{K}\sum_{k=1}^{K}\left(\hat{r}(k) - r(k)\right)^2}, \tag{25}$$

where $\hat{r}(k)$ is the model-predicted RSS at the time instance k, and $r(k)$ is the measured or observed RSS. For the TX-RX scheme measurements, the RMSE between the 3SM (blue dash line) and observations (canyon circles) is 2.17 dB. For the BC scheme measurements, the RMSE between the 3SM-BC (black line) and observation (red circles) is 2.94 dB. The relatively higher RMSE in the BC scenario might result from the more complicated propagation environment, non-strictly identical gait speeds and postures of the person in each measurement. The results indicate that both the 3SM and 3SM-BS can predict the RSS variations in their respective scenarios.

Moreover, as an essential indicator of human motion, RSS variance has been widely used by the RTI methods [18], [19] for device-free localization and tracking. In such cases, larger human motion-induced RSS variances can benefit localization accuracy. The RSS variance is expressed by

$$\sigma^2 = \frac{1}{K-1}\sum_{k=1}^{K}\left(r(k) - \overline{r}\right)^2, \tag{26}$$

where $\overline{r}$ is the mean of RSS. For the measurements in Fig. 5b, the human-induced RSS variance in the BC measurements is 29.51, whereas the value is only 9.92 in the TX-RX measurements. Therefore, the proposed BC scheme can benefit the variance-based RTI methods more than the TX-RX scheme.

The proposed model for the BC scenario is capable of capturing large RSS losses when the person is blocking the $\mathrm{LoS_{BC}}$ and capturing RSS variations resulting from reflection when the person is approaching the $\mathrm{LoS_{BC}}$. The model counts multiple reflections and attenuation caused by the backscatter propagation instead of the single TX-RX link in the referred models. Further, excess path lengths and their related human positions can be inferred from the RSS measurements.

V. Conclusion

We model the impact of a human on the RSS measurements in an indoor BC scenario represented by the three states. The RSS model 3SM-BC is derived and validated by measurements in an indoor corridor and is compared with 3SM in the conventional TX-RX scenario. The measurement shows that the 3SM-BC well predicts the RSS variation. It also shows that the human-induced RSS variation has a higher variance in the BC scenario, implying the advantage of BC-enabled sensing. The model facilitates BC-enabled sensing systems for human detection and localization. In a practical ISAC system, one can deploy multiple BDs at different locations, and hence cover a large sensitivity area. By applying the proposed RSS model to measurements from different BDs, as well as commonly used inference algorithms such as RTI and Bayesian filtering, we can implement device-free localization and human presence detection in the future ISAC system.

Acknowledgment

The authors appreciate Ruifeng Duan, Jari Lietzén, Lauri Mela, and Viktor Nässi for their support in discussions. This work is based upon the work part of BESIMAL project supported by the Academy of Finland under Grant 334197.

References

[1] Y. Cui, F. Liu, X. Jing, and J. Mu, “Integrating sensing and communications for ubiquitous IoT: Applications, trends, and challenges,” *IEEE Network*, vol. 35, no. 5, pp. 158–167, 2021.

[2] F. Adib and D. Katabi, “See through walls with WiFi!” in *Proceedings of the ACM SIGCOMM 2013*. New York, NY, USA: Association for Computing Machinery, 2013, p. 75–86.

[3] S. Yang and Y. Kim, “Single 24-GHz FMCW radar-based indoor device-free human localization and posture sensing with CNN,” *IEEE Sensors Journal*, vol. 23, no. 3, pp. 3059–3068, 2023.

[4] Y. Ma, Y. Zhang, B. Wang, and W. Ning, “SCLA-RTI: A novel device-free multi-target localization method based on link analysis in passive UHF RFID environment,” *IEEE Sensors Journal*, vol. 21, no. 3, pp. 3879–3887, 2021.

[5] H. Zhang, B. Di, K. Bian, Z. Han, H. V. Poor, and L. Song, “Toward ubiquitous sensing and localization with reconfigurable intelligent surfaces,” *Proceedings of the IEEE*, vol. 110, no. 9, pp. 1401–1422, 2022.

[6] 3GPP, “Study on ambient power-enabled Internet of Things,” 3rd Generation Partnership Project (3GPP), Technical Specification TS 22.840, Jun. 2023, version 1.2.0.

[7] 3GPP, “Study on ambient IoT (Internet of Things) in RAN,” 3rd Generation Partnership Project (3GPP), Technical Specification TS 38.848, Jun. 2023, version 0.2.0.

[8] N. Patwari and J. Wilson, “Spatial models for human motion-induced signal strength variance on static links,” *IEEE Transactions on Information Forensics and Security*, vol. 6, no. 3, pp. 791–802, 2011.

[9] R. Duan, X. Wang, H. Yiğitler, M. U. Sheikh, R. Jäntti, and Z. Han, “Ambient backscatter communications for future ultra-low-power machine type communications: Challenges, solutions, opportunities, and future research trends,” *IEEE Communications Magazine*, vol. 58, no. 2, pp. 42–47, 2020.

[10] V. Rampa, G. G. Gentili, S. Savazzi, and M. D'Amico, “Electromagnetic models for passive detection and localization of multiple bodies,” *IEEE Transactions on Antennas and Propagation*, vol. 70, no. 2, pp. 1462–1475, 2022.

[11] Y. Guo, K. Huang, N. Jiang, X. Guo, Y. Li, and G. Wang, “An exponential-rayleigh model for RSS-based device-free localization and tracking,” *IEEE Transactions on Mobile Computing*, vol. 14, no. 3, pp. 484–494, 2015.

[12] O. Kaltiokallio and H. Yiğitler, “Movement detection using a reciprocal received signal strength model,” in *IEEE ICASSP*, 2021, pp. 8318–8322.

[13] O. Kaltiokallio, H. Yiğitler, and R. Jäntti, “A three-state received signal strength model for device-free localization,” *IEEE Transactions on Vehicular Technology*, vol. 66, no. 10, pp. 9226–9240, 2017.

[14] Q. Tao, C. Zhong, K. Huang, X. Chen, and Z. Zhang, “Ambient backscatter communication systems with MFSK modulation,” *IEEE Transactions on Wireless Communications*, vol. 18, no. 5, pp. 2553–2564, 2019.

[15] N. Patwari and J. Wilson, “RF sensor networks for device-free localization: Measurements, models, and algorithms,” *Proceedings of the IEEE*, vol. 98, no. 11, pp. 1961–1973, 2010.

[16] B. Badihi, A. Liljemark, M. U. Sheikh, J. Lietzén, and R. Jäntti, “Link budget validation for backscatter-radio system in sub-1GHz,” in *IEEE WCNC*, 2019, pp. 1–6.

[17] S. Sankaralingam and B. Gupta, “Determination of dielectric constant of fabric materials and their use as substrates for design and development of antennas for wearable applications,” *IEEE Transactions on Instrumentation and Measurement*, vol. 59, no. 12, pp. 3122–3130, 2010.

[18] Y. Zhao and N. Patwari, “Robust estimators for variance-based device-free localization and tracking,” *IEEE Transactions on Mobile Computing*, vol. 14, no. 10, pp. 2116–2129, 2015.

[19] J. Wilson and N. Patwari, “See-through walls: Motion tracking using variance-based radio tomography networks,” *IEEE Transactions on Mobile Computing*, vol. 10, no. 5, pp. 612–621, 2011.